Transactions C: Chemistry and Chemical Engineering
Vol. 16, No. 2, pp. 108–124

SCIENTIA IRANICA

Mathematical Modeling of a Non-Catalytic Gas-Solid Reaction: Hematite Pellet Reduction with Syngas

M.S. Valipour[1]

Abstract. *A mathematical model is developed to investigate the nonisothermal reduction of the hematite pellet with Syngas, namely is a mixture of hydrogen, water vapour, carbon dioxide and carbon monoxide gases. This model is based upon special application of the grain model and contains the interactions between Syngas and the hematite pellet as a reflection of the heat and mass transfer phenomena. Each grain is reduced as an un-reacted shrinking core model at three interfaces simultaneously. A concluded set of equations is solved using the finite volume approach as an implicit formulation. Finally, the model was applied to study the isothermal and non-isothermal reduction of the hematite pellet and investigate the effects of Syngas characteristics, like gas utility ($(CO+H_2)/(CO_2+H_2O)$) and gas ratio (H_2/CO), on the rate of reduction.*

Keywords: *Mathematical modeling; Gas-solid reaction; Direct reduction iron; Hematite pellet; Kinetics.*

INTRODUCTION

The obvious industrial significance of iron oxide reduction by a reducing agent has stimulated a great deal of attention during the past three decades. Developments in this field of study have been consistently progressed to advance knowledge of the kinetics of the reduction process. A review of previous studies is briefly described in Table 1. These investigations may be categorized, based upon the methodology of study, into two groups: experimental-analytical modeling and mathematical modeling.

Experimental-analytical modeling: McKewan [1-3] has carried out an extensive experimental investigation on determining the rate controlling mechanism, using hydrogen as the reducing gas. He has then concluded that the overall rate of reduction may be controlled by interfacial chemical reactions. Afterward, he analytically rendered a correlation between the time characteristic and overall reduction rate, based on the Un-reacted Shrinking Core Model (USCM) in the Pseudo Steady State (PSS) condition. Turkdogan and Vinters [4,5] and Turkdogan et al. [6] have reported another wide experimental study on the reduction of the hematite pellet by hydrogen. They found that three major limiting rate controlling processes may exist during the reduction of iron ore, namely uniform internal reduction, limiting mixed control and gas diffusion in a porous iron layer. Szekely and El-Tawil [7] have reported preliminary measurements on the reduction of hematite disks with a mixture of hydrogen and carbon monoxide. They have observed that the required time to attain a given extent of reduction, markedly depends on the composition of the reducing gas. Furthermore, a comprehensive experimental and analytical study on the reduction of the hematite pellet with hydrogen or a mixture of carbon monoxide and hydrogen has been reported by Towhidi and Szekely [8,9]. They have indicated that the overall rate may be controlled by diffusion or a chemical reaction, depending on the temperature and the particle size. They also found that carbon deposition may occur during the reduction, with a mixture of carbon monoxide and hydrogen, when the operating temperature of the system is under 900°C. However, at higher temperatures and at high hydrogen content of reducing gas, the carbon deposition will be decreased. The effects of isothermality on the kinetics of iron ore reduction have been ex-

1. *Department of Mechanical Engineering, Faculty of Engineering, Semnan University, Semnan, P.O. Box 35196-45399, Iran. E-mail: msvalipour@semnan.ac.ir*

Received 23 July 2008; received in revised form 13 April 2009; accepted 28 June 2009

Table 1. Summary of the previous studies on the gaseous reduction of the hematite pellet.

Authors	Type of Study (Anal./Exp./Math.)	State (PSS/USS)	Isothermaity (NON/ISO)	Reducing Gas	Model
McKewan [1-3]	Exp. & Anal.	PSS	ISO	H_2	USCM
Spitzer et al. [16]	Math.	PSS	ISO	H_2-H_2O	USCM (dense pellet)
Spitzer et al. [17]	Math.	PSS	ISO	H_2-H_2O, H_2, H_2-N_2, H_2-He	3-interface USCM
Turkdogan and Vinters [4,5]	Exp. & Anal.	PSS	ISO	H_2	USCM
Tien and Turkdogan [18]	Math.	PSS	ISO	H_2-H_2O, CO-CO_2	Zone Model
Szekely and El-Tawil [7]	Exp.	PSS	ISO	H_2-CO	-
Tsay et al. [19]	Math.	PSS	ISO	H_2-CO	3-interface USCM
Hara et al. [20]	Math.	PSS	ISO	H_2-CO	3interface USCM
Yu and Gillis [22]	Math.	PSS	ISO	H_2-H_2O-N_2, CO-CO_2-N_2	Homogeneous
Towhidi and Szekely [8]	Exp. & Anal.	PSS	ISO	H_2, H_2-CO	USCM
Towhidi and Szekely [9]	Exp.	PSS	ISO	H_2, H_2-CO, H_2-CO-N_2	-
Negri et al. [21]	Math.	PSS	ISO	H_2-CO	3-interface USCM
Usui et al. [23]	Math./Exp.	PSS/USS	ISO	H_2-H_2O	Zone/Grain Model
Paul and Mukherjee [10]	Exp./Anal.	PSS	ISO/NON	CO	USCM
Proctor et al. [11]	Exp./Anal.	PSS	ISO	H_2-H_2O-CO-CO_2	USCM
Janowski and Sadowski [12]	Exp./Anal.	PSS	ISO	CO-CO_2	CCM/USCM
Moon et al. [13]	Exp./Anal.	PSS	ISO	H_2-CO	USCM
Kang et al. [14,15]	Exp./Anal.	PSS	ISO	CO-CO_2	USCM/Zone Model
Valipour et al. [26]	Math.	USS	NON	H_2-CO	Grain Model
Valipour and Saboohi [28]	Math.	USS	NON	H_2-CO-CO_2-H_2O	Grain Model
Bonalde et al. [24]	Exp./Math.	PSS	ISO	H_2-CO-CO_2-CH_4, H_2, CO	Grain Model
Valipour et al. [27]	Math.	USS	ISO	H_2-CO-CO_2-H_2O	Grain Model

perimentally investigated by Paul and Mukherjee [10]. They have specified that the nonisothermal reduction kinetics of iron ore pellets are a mixed controlled mechanism of three dimensional geometry controlling and the first order reaction. However, in the isothermal case, the reduction rate is controlled only by diffusion. Proctor et al. [11] have accomplished an experimental investigation on the reduction of the hematite pellet with a gaseous mixture of H_2-H_2O-CO-CO_2. They have claimed that the rate of reduction depends on the pellet oxygen content, the reduction potential of the gas phase, the temperature, the physical characteristics of the ore and the structural changes during the reduction. They have supposed that neither chemical control nor diffusion control is sufficient to describe the complete course of reduction alone. Janowski and Sadowski [12] have investigated the kinetics of hematite to magnetite reduction, in terms of physical changes in

the reducing oxide at low temperatures. Also, they have analytically investigated reduction kinetics using the Crackling Core Model (CCM). Moon et al. [13] have experimentally investigated the reduction behavior of the hematite compacts with a mixture of hydrogen and carbon monoxide at 800-900°C. They have analytically discussed that the reduction could not be described in terms of a single rate determining step. The reduction process is initially controlled by the chemical reaction at the oxide/iron interface; it is mixed controlled at the intermediate reduction time and will be controlled by intraparticle diffusion through the reduced layer towards the end of the reduction. The effects of iron ore shape and size on the reduction rate have been investigated experimentally and analytically by Kang et al. [14,15]. They have found that the reduction rate increases with decreasing the particle size and, for non-spherical particles, the reduction rate becomes faster as the non-spherical radius becomes smaller.

Mathematical Modeling: In spite of the wide experimental studies, there is not a complete kinetic law that can well describe the reduction process of the hematite pellet alone. The major reason of this shortcoming is the complexity of the reduction process due to the diversity of the effective parameters. So, the experimental analysis is not alone appropriate for estimating the kinetics of the hematite reduction. This shortcoming of experimental studies has led investigators to apply mathematical models for the reason that mathematical models not only can easily deal with complex systems of reduction, but can also reduce the cost of experimental study very well. The mathematical models themselves can be considered as one or three interface USCM. Zone model, Homogeneous model and Grain model.

Spitzer et al. [16,17] have introduced mathematical models to describe the reduction kinetics of the dense pellet and the porous pellet of iron oxide with hydrogen. For developing the model, they have used one interface USCM for the dense pellet and three interface USCM (hematite-magnetite, magnetite-wustite, wustite-iron) for the porous pellet. Tien and Turkdogan [18] have developed a PSS and isothermal mathematical formulation, based on experimental observations, as a zone model for investigating the reduction process with hydrogen or with carbon monoxide. Tsay et al. [19] have developed a generalization of the Spitzer model for two reactant gas mixtures including hydrogen and carbon monoxide. Hara et al. [20] have developed the three interface USCM to describe the kinetics of porous pellet reduction in three steps, simultaneously. Negri et al. [21] have presented a generalization of the Hara model for porous pellet reduction, based on the three interface model, as a matrix form. They have also considered a different diffusivity and mass transfer coefficient for reactants and products. Yu and Gillis [22] have studied PSS reduction of the hematite with hydrogen or carbon monoxide, using a homogeneous model in the pellet scale.

Usui et al. [23] have investigated the isothermal reduction of the wustite pellet with hydrogen, based on the grain model, as pseudo steady state and unsteady state conditions. They have indicated that the PSS solution of their model had a good accuracy when compared with the USS solution. The kinetics of the reduction of the hematite pellet using a Midrex gas composed of CO, H_2, CH_4 and CO_2 was investigated by Bonalde et al. [24], based on the isothermal PSS grain model. They found that the reduction of iron oxide pellets using Midrex gas is a mixed-controlled system throughout the whole reduction process.

This introduction obviously indicated that the practical application of previous studies on iron ore reduction has been restricted by some simplifications, such as isothermal condition, pseudo steady state condition and simple reducing gas (see Table 1). Generally, these conditions are different from conditions prevalent in industrial practices. In this paper, a nonisothermal, unsteady mathematical model of the reduction process on the pellet scale which can deal with a multi-component reducing gas is presented to overcome the shortcomings of previous studies. This general model is based upon the three-interface application of the grain model, which has been primarily reported by Szekely and Evans [25]. As discussed in previously presented papers by the authors [26-28], a fully implicit finite volume approach is employed for the solution of model equations to prevent numerical instability and to shorten computation time.

MATHEMATICAL FORMULATION

Concepts and Assumptions

Figure 1 shows a schematic representation of a hematite porous pellet that is reduced to sponge iron with

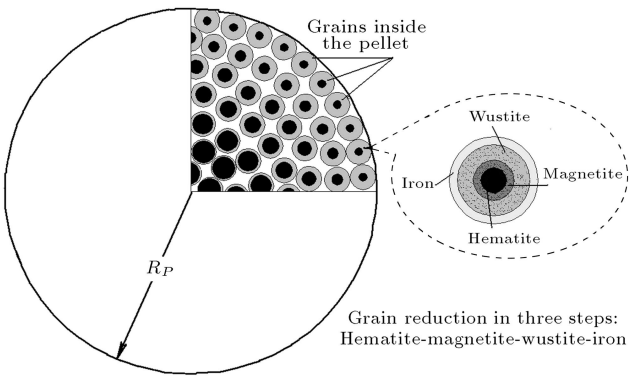

Figure 1. Schematic representation of the pellet reduction as a grain model at three interfaces.

Syngas, namely a gaseous mixture of hydrogen, water vapour, carbon monoxide and carbon dioxide. Generally, the hematite pellet composed of dense small grains is reduced to iron in a series of consecutive reactions; above 560°C, hematite → magnetite → wustite → iron; below 560°C, wustite is unstable, so the reaction proceeds as hematite → magnetite → iron [22]. The reduction process may be controlled by mass transfer between the pellet surface and the bulk gas stream by gaseous diffusion through the pellet, by the chemical reaction rate or by any combination of these controlling processes, depending upon the values of various parameters. The generation and consumption of heat by reactions, heat transfer by effective conduction and heat exchange with the external environment are the phenomena that may affect temperature distribution inside the pellet. The particular reaction system that will be treated here is a set of consecutive reactions as follows:

$$3Fe_2O_3 + H_2 \text{ (or CO)} = 2Fe_3O_4 + H_2O \text{ (or } CO_2), \quad (1)$$

$$\frac{w}{4w-3}Fe_3O_4 + H_2 \text{ (or CO)} = \frac{3}{4w-3}Fe_wO + H_2O \text{ (or } CO_2), \quad (2)$$

$$Fe_wO + H_2 \text{ (or CO)} = wFe + H_2O \text{ (or } CO_2), \quad (3)$$

where w is the atomic ratio of iron to oxygen in wustite and is shown to vary from $w = 0.95$ along the wustite-iron boundary to $w = 0.85$ along the wustite-magnetite boundary at atmospheric pressure [22].

The development and formulation of the mathematical model has been based on the following assumptions:

- The pellet is spherical and is composed of dense hematite micro-grains having a small constant radius.
- The reaction of the grains is reversible, is of first order and it proceeds topochemically.
- The reacting system of each grain includes three steps, i.e. converting hematite to magnetite, magnetite to wustite and wustite to iron.
- During the reduction in the pellet, the diameter is not changed and the cracks are not formed.
- The regime is transient and not pseudo-steady state.
- The compositions and temperature of the bulk stream may be varied as a function of time.
- Catalytic effects may be neglected and the effect of the water gas shift reaction ($CO+H_2O=CO_2+H_2O$) may also be neglected.

Governing Equations

Reaction Rate Modeling

It is assumed that the chemical reaction and the gaseous diffusion proceed simultaneously in the pellet, which is composed of small grains. Therefore, the reduction nearly proceeds homogeneously in a macroscopic view. The microscopic view of the grain reduction has been envisaged topochemically as USCM at three interfaces, simultaneously. Therefore, the chemical reaction rate of a grain with a reducing gas is given as follows:

$$\dot{v}_{h,i} = \frac{C_t^b}{W_{3,i}} \left[\begin{array}{l} \{A_3(A_2+B_2+B_3+F) \\ \quad +(A_2+B_2)(B_3+F)\}(Y-Y_{eh}) \\ -\{B_2(A_3+B_3+F) \\ +A_3(B_3+F)\}(Y-Y_{em}) \\ -\{A_2(B_3+F)\}(Y-Y_{ew}) \end{array} \right]_i, \quad (4)$$

$$\dot{v}_{m,i} = \frac{C_t^b}{W_{3,i}} \left[\begin{array}{l} -\{B_2(A_3+B_3+F) \\ \quad +A_3(B_3+F)\}(Y-Y_{eh}) \\ +\{(A_1+B_1+B_2)(A_3+B_3+F) \\ +A_3(B_3+F)\}(Y-Y_{em}) \\ -\{(A_1+B_1)(B_3+F)\}(Y-Y_{ew}) \end{array} \right]_i, \quad (5)$$

$$\dot{v}_{h,i} = \frac{C_t^b}{W_{3,i}} \left[\begin{array}{l} -\{A_2(B_3+F)\}(Y-Y_{eh}) \\ -\{(A_1+B_1)(B_3+F)\}(Y-Y_{em}) \\ +\{(A_1+B_1)(A_2+B_2+B_3+F) \\ \quad +A_2(B_2+B_1+F)\}(Y-Y_{ew}) \end{array} \right]_i, \quad (6)$$

$$W_{3,i} = \left[\begin{array}{l} (A_1+B_1)\{A_3(A_2+B_2+B_3+F) \\ \quad +(A_2+B_2)(B_3+F)\} \\ +A_2\{A_3(B_2+B_3+F)\} \\ +\{B_2(B_3+F)\} \end{array} \right]_i, \quad (7)$$

$$A_{1,i} = \left[\frac{1}{(1-f_h)^{\frac{2}{3}}} \frac{1}{k_{rh}\left(1+\frac{1}{Ke_h}\right)} \right]_i, \quad (8)$$

$$A_{2,i} = \left[\frac{1}{(1-f_m)^{\frac{2}{3}}} \frac{1}{k_{rm}\left(1+\frac{1}{Ke_m}\right)} \right]_i, \quad (9)$$

$$A_{3,i} = \left[\frac{1}{(1-f_w)^{\frac{2}{3}}} \frac{1}{k_{rw}\left(1+\frac{1}{Ke_w}\right)} \right]_i, \quad (10)$$

$$B_{1,i} = \left[\frac{(1-f_m)^{\frac{1}{3}} - (1-f_h)^{\frac{1}{3}}}{(1-f_h)^{\frac{1}{3}}(1-f_m)^{\frac{1}{3}}} \frac{r_g}{D_{eh}} \right]_i, \quad (11)$$

$$B_{2,i} = \left[\frac{(1-f_w)^{\frac{1}{3}} - (1-f_m)^{\frac{1}{3}}}{(1-f_m)^{\frac{1}{3}}(1-f_w)^{\frac{1}{3}}} \frac{r_g}{D_{em}} \right]_i, \quad (12)$$

$$B_{3,i} = \left[\frac{1-(1-f_w)^{\frac{1}{3}}}{(1-f_w)^{\frac{1}{3}}} \frac{r_g}{D_{ew}} \right]_i, \quad (13)$$

$$F_i = \left[\frac{1}{k_f} \right]_i, \quad (14)$$

where i is related to the reducing agents (H_2, CO).

The local fractional reduction of each ore species in the three interface model, as shown in Figure 1, is calculated as:

$$\frac{\partial f_l}{\partial t} = \sum_{i=\mathrm{CO},\mathrm{H_2}} \frac{3(1-\varepsilon)}{r_g} \left(\frac{\dot{v}_{l,i}}{d_{O,l}} \right), \quad (15)$$

$$f_l = 1 - \left(\frac{r_l}{r_g} \right)^3, \qquad l = h, m, w, \quad (16)$$

where the total local fractional reduction, f, is calculated as the following relationship, which indicates the reducible oxygen content at each stage of reduction [20]:

$$f = \alpha_h f_h + \alpha_m f_m + \alpha_w f_w. \quad (17)$$

The overall fractional reduction of the pellet may be estimated as an integration of f over the entire pellet as follows:

$$F = \frac{3}{R_P^3} \int_0^{R_P} r^2 f dr. \quad (18)$$

Equation of Energy

Heat transfer in porous media should include conduction, radiation and convection terms. The relative importance of these mechanisms varies depending on solid properties, pore structure, temperature range and gas flow in each case. Shi et al. [29] have reported that the effect of the convection term due to gas movement within the pellet is negligible. By considering an effective thermal conductivity, containing radiant and conductive terms, the heat transfer may be written as follows [28]:

$$(\rho C_P)_{\mathrm{eff}} \frac{\partial T}{\partial t} = \nabla.(\lambda_{\mathrm{eff}} \nabla T) + \sum_{i=\mathrm{CO},\mathrm{H_2}} \sum_{l=h,m,w} \frac{3(1-\varepsilon)}{r_g} \dot{v}_{i,l} (-\Delta H)_{T,i,l}, \quad (19)$$

where $(-\Delta H)_{T,i,j}$ represents heat generation or consumption by chemical reactions of species i at interface l.

Continuity Equation of Species

The following phenomena should be considered to develop the mass equation of the gaseous species within the pellet:

- Convective mass transfer of the gaseous species from bulk flow to the pellet surface.
- Diffusion of the gaseous species within the pores of the pellet.
- Chemical reaction with the solid reactant at the solid interfaces inside each grain.
- Diffusion of the product away from the reaction surface through the solid porous layer.
- Convective mass transfer of the product through the gas film surrounding the solid pellet into the bulk flow.

Therefore, the continuity of gaseous species yields a mass equation for the gaseous reactant and product species as follows:

$$\frac{\partial(\varepsilon C_i)}{\partial t} = \nabla.(D_{\mathrm{eff},i} \nabla C_i) + \sum_l \nu_{li} \frac{3(1-\varepsilon)}{r_g} \dot{v}_{i,l}, \quad (20)$$

where ν_{li} is the stoichiometric coefficient for species i appearing in the lth reaction interface. For the reactant species it has a positive value, $\nu_{li} > 0$. On the other hand, for the products it has a negative value, $\nu_{li} < 0$.

Auxiliary Equations

Some additional relationships are required for solving the set of equations which are mentioned above. These are as follows:

$$\sum_i Y_i = 1.0, \quad (21)$$

$$C_i = Y_i C_t, \quad (22)$$

$$C_t = \frac{P_t}{R_G T}. \quad (23)$$

Initial and Boundary Conditions

The temperature and chemical composition of the bulk flow may be varied as a function of time. Hence, for the continuity of heat and mass fluxes on the surface of the pellet, $r = R_P$, we have:

$$-\lambda_{\mathrm{eff}} \frac{\partial T(R_P,t)}{\partial r} = h(T_s(R_P,t) - T_b), \quad (24)$$

$$-D_{\mathrm{eff},i} \frac{\partial C_i(R_P,t)}{\partial r} = k_{m,i}(C_{s,i}(R_P,t) - C_{b,i}). \quad (25)$$

Due to the spherical symmetry at the centre of the pellet, $r = 0$;

$$\frac{\partial T(0,t)}{\partial r} = 0, \quad (26)$$

$$\frac{\partial C_i(0,t)}{\partial r} = 0, \quad (27)$$

and the initial conditions at $t = 0$ are:

$$T(r,0) = T_0, \tag{28}$$

$$C_i(r,0) = C_{i,0}, \tag{29}$$

$$f_l(r,0) = f_{l,0}. \tag{30}$$

EXPRESSION OF THE PARAMETERS

Basically, the thermo-physical and thermo-chemical parameters involved in the previous equations are functions of temperature, pressure and chemical composition. However, they have been frequently considered constant in previous works [7,10,11,20,22,24] . Here, assessment of these parameters will be explained.

Mass Transfer Coefficients

$k_{f,i}$, the mass transfer coefficient for each species, and h, the heat transfer coefficient for the bulk flow, are estimated from classical correlations, expressing Sherwood or Nusselt numbers as a function of Reynolds, Schmidt or Prandtl numbers. For a single pellet the following correlations have been proposed [30]:

$$\mathrm{Sh}_i = 2 + 0.6\ \mathrm{Re}_P^{\frac{1}{2}}\ \mathrm{Sc}_i^{\frac{1}{3}}, \tag{31}$$

$$\mathrm{Nu} = 2 + 0.6\ \mathrm{Re}_P^{\frac{1}{2}}\ \mathrm{Pr}^{\frac{1}{3}}. \tag{32}$$

Effective Diffusivity

The diffusion of gaseous species through a porous solid depends on structure, void fraction, tortuosity factor and pore size distribution. When the pore diameter is large, compared with the mean free path of the gas molecules, molecular diffusion is predominant and molecular binary diffusivity is estimated by the use of the Fuller-Schettler-Giddings equation [31,32]:

$$D_{ij} = \frac{1 \times 10^{-7} T^{1.75}}{P_t \left(\bar{v}_i^{1/3} + \bar{v}_j^{1/3}\right)^2} \left(\frac{1}{M_i} + \frac{1}{M_j}\right)^{0.5}, \tag{33}$$

where $\bar{v}_i$ is the diffusion volume of the ith species which have been given in Table 2. for the species of the Syngas.

Conversely, in solids with fine pores the Knudsen diffusion mechanism prevails, but in pores with intermediate size a mixed type of diffusion may occur. In this situation the effective intraparticle diffusion of each gaseous species is obtained by the following correlation [28,33]:

$$\frac{1}{D_{\mathrm{eff},i}} = \frac{1}{D^K_{\mathrm{eff},i}} + \frac{1}{D^m_{\mathrm{eff},i}}, \tag{34}$$

where $D^K_{\mathrm{eff},i}$ and $D^m_{\mathrm{eff},i}$ are the effective Knudsen diffusion and the effective molecular diffusion of the ith species, respectively. The estimation of these effective diffusivities has been discussed in a previous paper by the authors [28].

Table 2. Diffusion volumes for some species [32].

Molecule	H_2	H_2O	CO	CO_2	N_2
$\bar{v}$	7.07	12.7	18.9	26.9	17.9

Effective Thermal Conductivity

The effective thermal conductivity of a porous pellet during the reduction process depends on the properties of the constituent solids and gases, the temperature and the porosity of the structure. The thermal conductivity of a gaseous mixture is calculated using the following relation [34]:

$$\lambda_g = \frac{\sum_i Y_i M_i^{\frac{1}{3}} \lambda_{gi}}{\sum_i Y_i M_i^{\frac{1}{3}}}, \tag{35}$$

where λ_i is the thermal conductivity of the ith component which is reported as a function of the temperature by Donskoi and McElwain [34].

The mean thermal conductivity of the solid structure has been estimated by the following formula [33,35]:

$$\lambda_s = \sum_j f_j \lambda_{sj}, \tag{36}$$

where λ_{sj} is the thermal conductivity of the solid component j and f_j is the volume fraction of the jth component of the solid. The thermal conductivity of the iron oxides (hematite, magnetite, wustite and iron) has been correlated as a function of the temperature by Akiyama et al. [35]. Therefore, the effective thermal conductivity can be obtained from the following relation, in which the arrangements of the solid matrix and pores are in parallel and in series [34,35]:

$$\lambda_{\mathrm{eff}} = \tfrac{1}{3}\left\{(1-\varepsilon)\lambda_s + \varepsilon\lambda_g\right\} + \tfrac{2}{3}\left\{(1-\varepsilon)/\lambda_s + \varepsilon/\lambda_g\right\}^{-1}. \tag{37}$$

Effective Heat Capacity

The effective heat capacity of a porous pellet during the reduction process depends on the properties of the constituent solids and gases, the temperature and the porosity structure. The specific heat of the multi-component gas mixture or solid matrix can be evaluated by the following formula [33,36]:

$$C_{P,j} = \left(\frac{\sum_i Y_i M_i C_{Pi}}{\sum_i Y_i M_i} \right)_j, \qquad j = s, g, \tag{38}$$

where C_{Pi} is the specific heat of each component, i, and has been also expressed as a function of the temperature by Donskoi and McElwain [34]. The effective heat capacity of the pellet as a porous medium is calculated as the following:

$$(\rho C_P)_{\text{eff}} = (1-\varepsilon)(\rho c)_s + \varepsilon(\rho c)_g. \tag{39}$$

Heat of Reactions

There are many articles in which the heat of reaction for the direct reduction of iron ore is estimated at room temperature (298.15 K). However, the heat of reaction usually depends on the temperature. Figure 2 shows that, at any temperature, the conversion of hematite to magnetite and the conversion of wustite to iron with carbon monoxide are exothermic reactions, but it is endothermic for the conversion of magnetite to wustite by carbon monoxide [33].

As shown in Figure 3, the conversion of magnetite to wustite and the conversion of wustite to iron with hydrogen are endothermic reactions at any temperature. However, hematite is reduced to magnetite as a weakly endothermic reaction in the temperature range 827.4 K $< T <$ 913.3 K, whereas at other temperatures it is reduced as an exothermic reaction [33].

Activation Energy, Frequency Factor and Equilibrium Constant

The activation energy and frequency factor that have been proposed by Tsay et al. [19] are applied to reactions 1 to 3. Frequency factor, activation energy and equilibrium constants for each reaction are listed in Table 3.

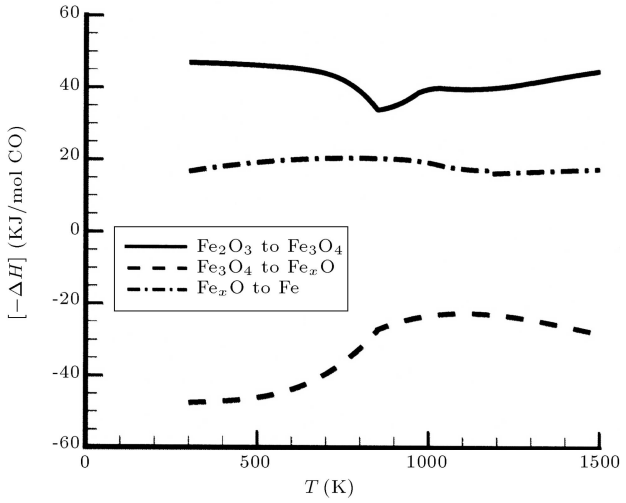

Figure 2. Heat of reactions versus temperature for iron oxide reduction by carbon monoxide.

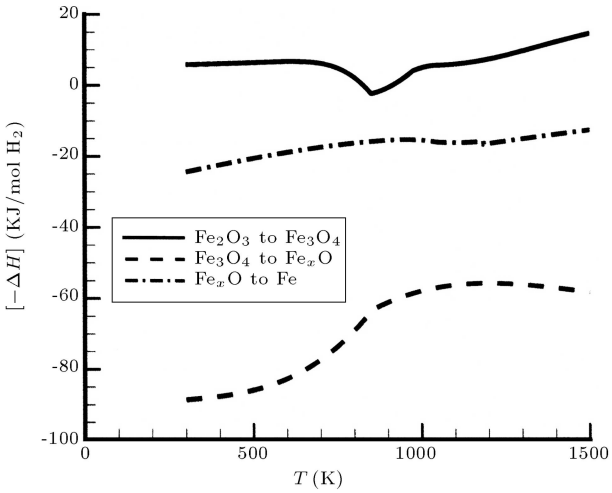

Figure 3. Heat of reactions versus temperature for iron oxide reduction by hydrogen.

Porosity

Porosity is an important physical property that may considerably affect the reduction process. In many previous works it has been considered as a constant. However, it changes during the reduction as a function of time and location. Here, it is linearly correlated, based on the experimental data of Akiyama et al. [35] as follows:

$$\begin{aligned}
&\varepsilon = \varepsilon_0 + \eta_h (f - f_0), \\
&f_0 < f \leq f_1 (= \alpha_h), \\
&\varepsilon = \varepsilon_m + \eta_m (f - f_1), \\
&f_1 < f \leq f_2 (= \alpha_h + \alpha_m), \\
&\varepsilon = \varepsilon_w + \eta_w (f - f_2), \\
&f_2 < f < 1,
\end{aligned} \tag{40}$$

where f_1 and ε_m are the local reduction rate and the local porosity, respectively, when the hematite is completely reduced to magnetite. f_2 and ε_m are the local reduction rate and the local porosity when the magnetite is totally reduced to wustite. η_h, η_m and η_w are empirical coefficients, which are listed in Table 4 for different types of pellet.

NUMERICAL SOLUTION

To solve the complicated governing equations, they are rendered discrete using the finite volume approach with a fully implicit formulation. As explained in

Table 3. Frequency factor, activation energy and equilibrium constant of reactions 1 to 3.

	k_0 (m/s)	E_a ($\frac{kJ}{mol}$)	Ke
$3Fe_2O_3 + H_2 \rightarrow 2Fe_3O_4 + H_2O$	160	92.092	$\text{Exp}\left(\frac{-362.6}{T} + 10.334\right)$
$\frac{w}{4w-3}Fe_3O_4 + H_2 = \frac{3}{4w-3}Fe_wO + H_2O$	23	71.162	$\text{Exp}\left(\frac{-7916.6}{T} + 8.46\right)$
$Fe_wO + H_2 \rightarrow wFe + H_2O$	30	63.627	$\text{Exp}\left(\frac{-1586.9}{T} + 0.9317\right)$
$3Fe_2O_3 + CO \rightarrow 2Fe_3O_4 + CO_2$	2700	113.859	$\text{Exp}\left(\frac{3968.37}{T} + 3.94\right)$
$\frac{w}{4w-3}Fe_3O_4 + CO = \frac{3}{4w-3}\ Fe_wO + CO_2$	25	73.674	$\text{Exp}\left(\frac{-3585.64}{T} + 8.98\right)$
$Fe_wO + CO \rightarrow wFe + CO_2$	17	69.488	$\text{Exp}\left(\frac{2744.63}{T} - 2.946\right)$

Table 4. The coefficients of Equation 32 for different types of pellets.

	η_h	η_m	η_w
Fired pellet	0.75	0.8334	0.1667
Non-fired pellet	0.5	0.5834	0.1212
Sinter	1	0.5	0.091

the previous paper [27,28], this method reduces the differential equations to a large set of coupled linear algebraic equations that have been solved using an indirect iterative procedure as a TDMA (Tri-Diagonal Matrix Algorithm) method [37]. The fully implicit formulation has the advantage that the time increments required for its convergence are not too small. The methodology and algorithm of the solution have been exhaustively described in a previous paper by the authors [28].

RESULTS AND DISCUSSIONS

Validation

Upon formulation of the mathematical model, the validation of the model is set up and the overall reduction degree of the hematite fired pellet, F, has been studied as a validation parameter. The experimental results reported by Bonalde et al. [24] have been used for validation of the model estimations. The model is run to simulate the isothermal reduction process of pellet Type A with a physico-chemical description, like Table 5, in an atmosphere of pure H_2, pure CO and a mixture of H_2: 55.7%, H_2O: 4.0%, CO: 34.0% and CO_2: 6.3%, namely Syngas. A gas flow rate of 0.002 m^3/min is used in all the reduction cases.

Figure 4 shows a comparison between the experimental data reported by Bonalde et al. [24] and the predictions of the present model on the overall rate of reduction for pellet Type A. Figures 4a, 4b and 4c demonstrate the comparison for reduction with pure hydrogen, pure carbon monoxide and Syngas; a mixture of CO-CO_2-H_2-H_2O, respectively. They indicate a good agreement between the experimental data and the theoretical predictions in all three cases. In addition, detailed information of the three interface reduction model is plotted in Figures 4a, 4b and 4c where they demonstrate a detailed description of the rate of local reduction during the conversion of hematite to magnetite, magnetite to wustite and wustite to iron, in each case.

Isothermal Reduction

Depending on the pelletizing system, the size of pellets usually used in industrial direct reduction technologies

Table 5. Physical characteristic and chemical composition of the fired-pellet.

Type	d_P (mm)	ε_0	ρ_P (kg/m^3)	T.Fe	FeO	SiO_2	Al_2O_3	CaO	MgO	C	S
A	10.7	0.22	4700	67.64	0.58	1.28	0.64	1.0	0.36	0.01	5 ppm
B	18	0.22	4700	67.64	0.58	1.28	0.64	1.0	0.36	0.01	5 ppm

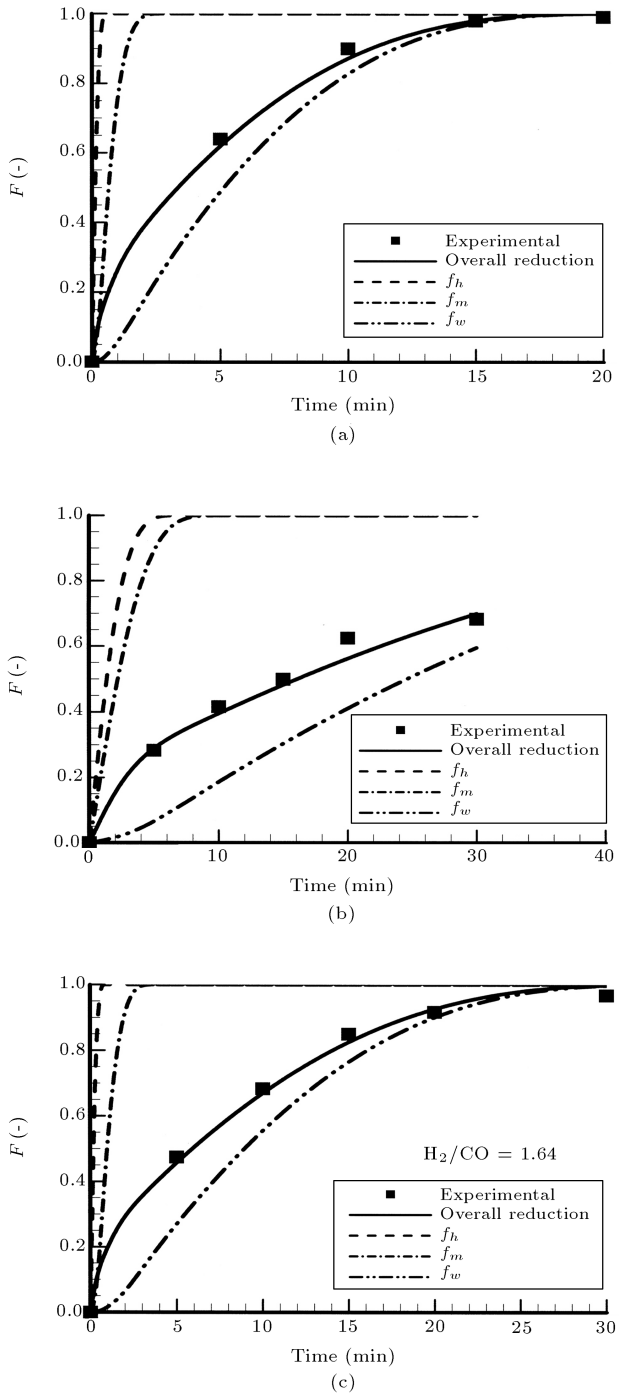

Figure 4. A comparison between the model estimations and the experimental data [24] for the pellet Type A in a bulk flow temperature $T_b = 1123$ K: (a) Reduction with pure hydrogen; (b) Reduction with pure carbon monoxide; (c) Reduction with Syngas.

is varied within the range of 5-18 mm. Hereafter, in our study, we will use pellet Type B, which is the largest size of pellet usually applied in industrial applications. The model is run to simulate the isothermal reduction of pellet Type B with pure hydrogen, pure carbon monoxide and a H_2/CO gas mixture. The results are plotted in Figures 5 to 7. It is indicated in Figures 5b, 6b and 7b that:

I. In spite of the isothermal reduction, the tempera-

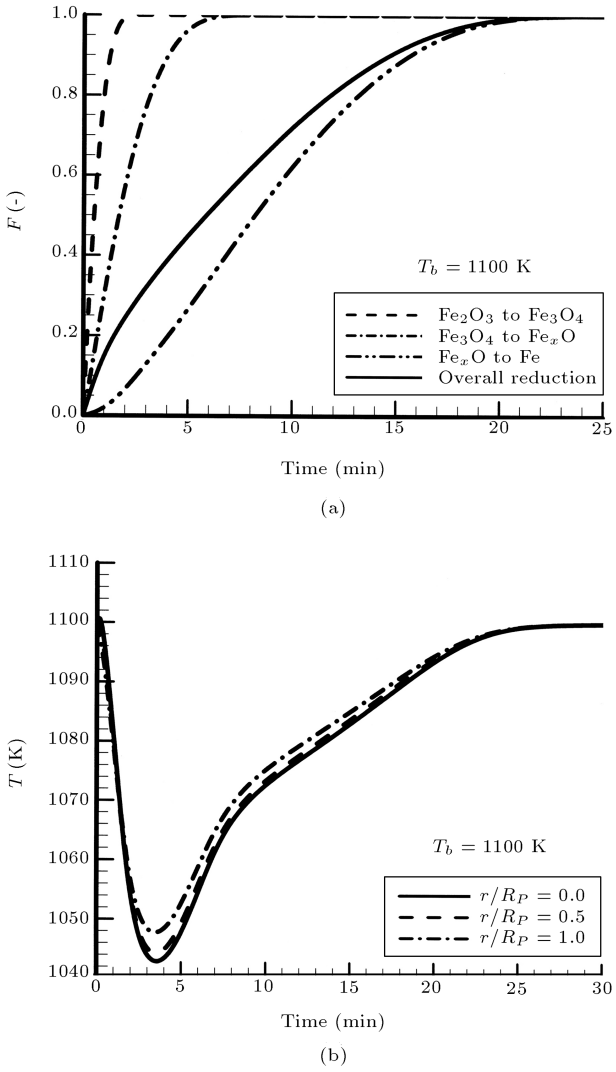

Figure 5. Isothermal reduction of the pellet Type B with pure hydrogen: (a) The overall reduction and the reduction of each iron oxide vs. time; (b) The temperature variation in three positions within the pellet vs. time.

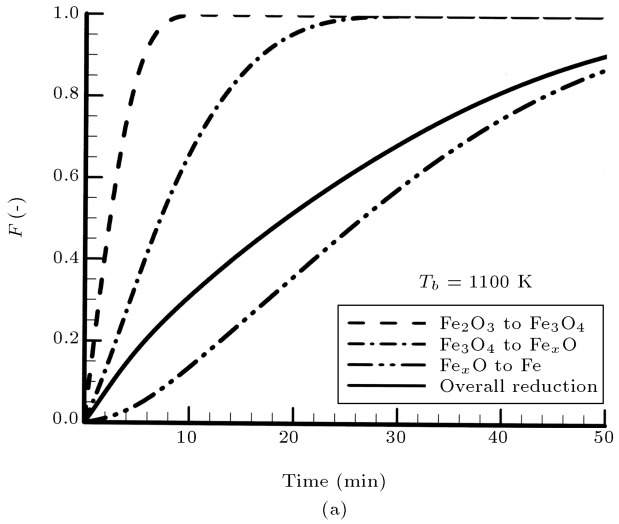

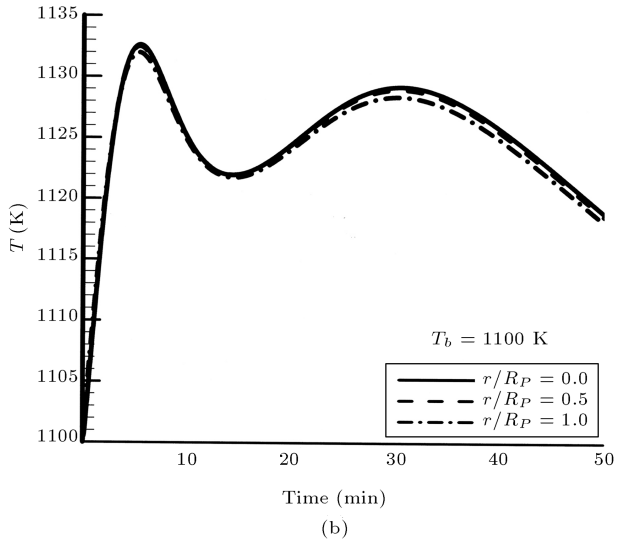

Figure 6. Isothermal reduction of the pellet Type B with pure carbon monoxide: (a) The overall reduction and the reduction of each iron oxide vs. time; (b) The temperature variation in three positions within the pellet vs. time.

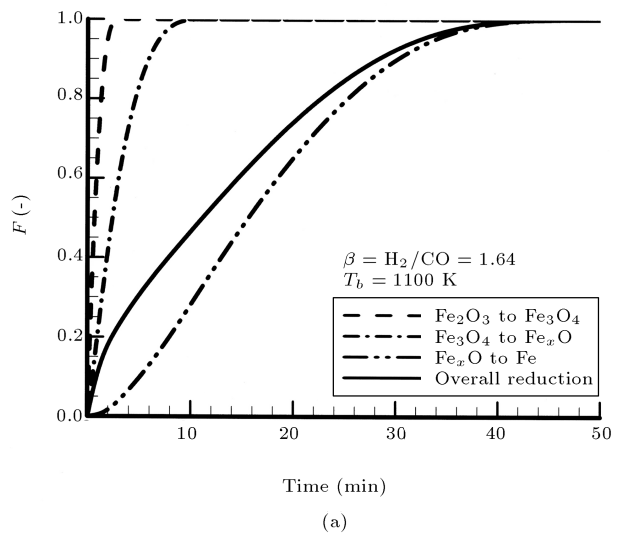

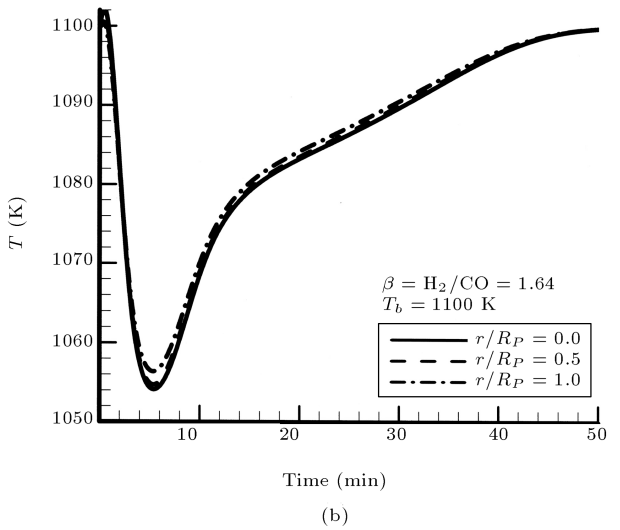

Figure 7. Isothermal reduction of the pellet Type B with Syngas: (a) The overall reduction and reduction of each iron oxide vs. time; (b) The temperature variation in three positions within the pellet vs. time.

ture within the pellet is varied during the reduction process.

II. Temperature variations of the three different positions inside the pellet are very close to each other.

This reveals that the temperature is only a function of time and is almost independent of the position inside the pellet during the reduction.

Furthermore, it can be seen that the temperature of the pellet decreases while the conversion of hematite to magnetite and magnetite to wustite are in progress. As shown in Figure 5, in the reduction with hydrogen, hematite is converted into magnetite very soon as an exothermic reaction, while magnetite is contemporarily reduced to wustite as a highly endothermic reaction. Hence the temperature of the pellet is reduced by 35% of the overall reduction (f_h = 1.0, f_m = 0.84, f_w = 0.16). Afterwards, the intensity of the endothermic reaction is decreased so that the temperature is locally increased due to a less endothermic reaction of wustite conversion with hydrogen. Then, the temperature is concurrently approached to the bulk flow temperature as the pellet is fully reduced to iron.

Figure 6a shows the reduction rate of pellet Type B with pure carbon monoxide and Figure 6b demonstrates the temperature variation at three points within the pellet during the reduction process. Despite the isothermal reduction, Figure 6b shows that the temperature within the pellet is varied while the reduction progresses. Also, it can be seen that the temperature of the pellet increases as far as until 18% of the pellet is reduced (f_h = 0.88, f_m = 0.37,

$f_w = 0.05$). This is due to the dominant effect of the highly exothermic conversion of hematite to magnetite with carbon monoxide (see Figure 3). Afterwards, the highly endothermic conversion of magnetite to wustite prevails, so the temperature is locally reduced by 40% of the overall reduction ($f_h = 1.0$, $f_m = 0.8$, $f_w = 0.23$). Also, the wustite is contemporarily reduced to iron as a highly exothermic reaction. Therefore, as the exothermic reduction of wustite to iron overcomes, accordingly the temperature is again increased by 70% of the overall reduction ($f_h = 1.0$, $f_m = 1.0$, $f_w = 0.57$). Then, the temperature will decline to approach the bulk flow temperature when the pellet is fully reduced to iron.

Figure 7 shows the model results for pellet Type B with syngas; a gaseous mixture including H_2: 55.7%, H_2O: 4.0%, CO: 34.0% and CO_2: 6.3% in which gas ratio ($\frac{H_2}{CO}$) is about 1.64. Despite the isothermal reduction process, Figure 7b shows that the temperature within the pellet is varied with the time of reduction. In this case, the temperature variation is similar to the case of reduction by hydrogen because of gas ratio ($\beta > 1.0$). The temperature of the pellet decreases until 32% of the pellet is reduced ($f_h = 1.0$, $f_m = 0.87$, $f_w = 0.11$). This is due to the prevailing effect of the endothermic reactions as the conversion of magnetite to wustite, which is endothermically reduced by carbon monoxide as well as hydrogen (see Figures 2 and 3). Afterwards, the intensity of the endothermic reactions declines because the concentration of magnetite is decreased within the pellet. So, the temperature will increase to approach the bulk temperature when the pellet is fully reduced to iron. It should be considered, however, that the wustite is endothermically reduced to iron by hydrogen, but is reduced to iron by carbon monoxide, exothermically.

Non-Isothermal Reduction

The model was run to simulate the non-isothermal reduction of pellet Type B in different reducing gases, namely pure hydrogen, pure carbon monoxide and Syngas. The gas ratio and gas utility of the Syngas are $\gamma = 1.64$ and $\beta = 8.71$, respectively.

Figures 8, 9 and 10 show the results of the nonisothermal reduction of pellet Type B using pure hydrogen, pure carbon monoxide and Syngas, respectively. In Figures 8a, 9a and 10a, the reduction rate of each iron oxide component, as well as the overall reduction rate, are shown. Figures 8b, 9b, 10a and 10b illustrate the gaseous reactant and products at $r = 0$, $r = R_P/2$ and $r = R_P$ within the pellet during the reduction process. Figures 8c, 9c and 10d illustrate the temperature variation at $r = 0$, $r = R_P/2$ and $r = R_P$ within the pellet during the reduction process. It is shown in Figures 8c, 9c

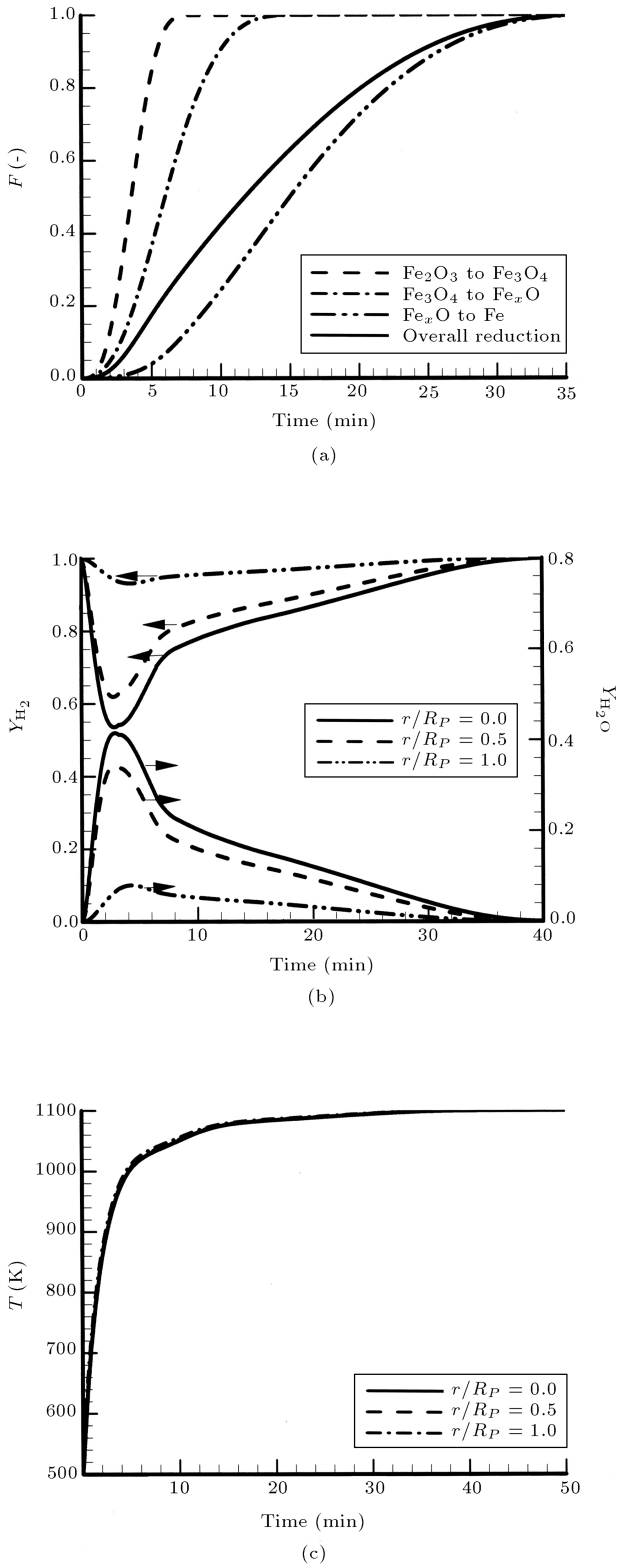

Figure 8. The model estimation for non-isothermal reduction of the pellet Type B with using pure hydrogen: (a) Overall reduction rate and reduction rate of each iron oxide component; (b) Gaseous reactant and product variation at three different positions within the pellet during the reduction; (c) Temperature variation at three different positions inside the pellet.

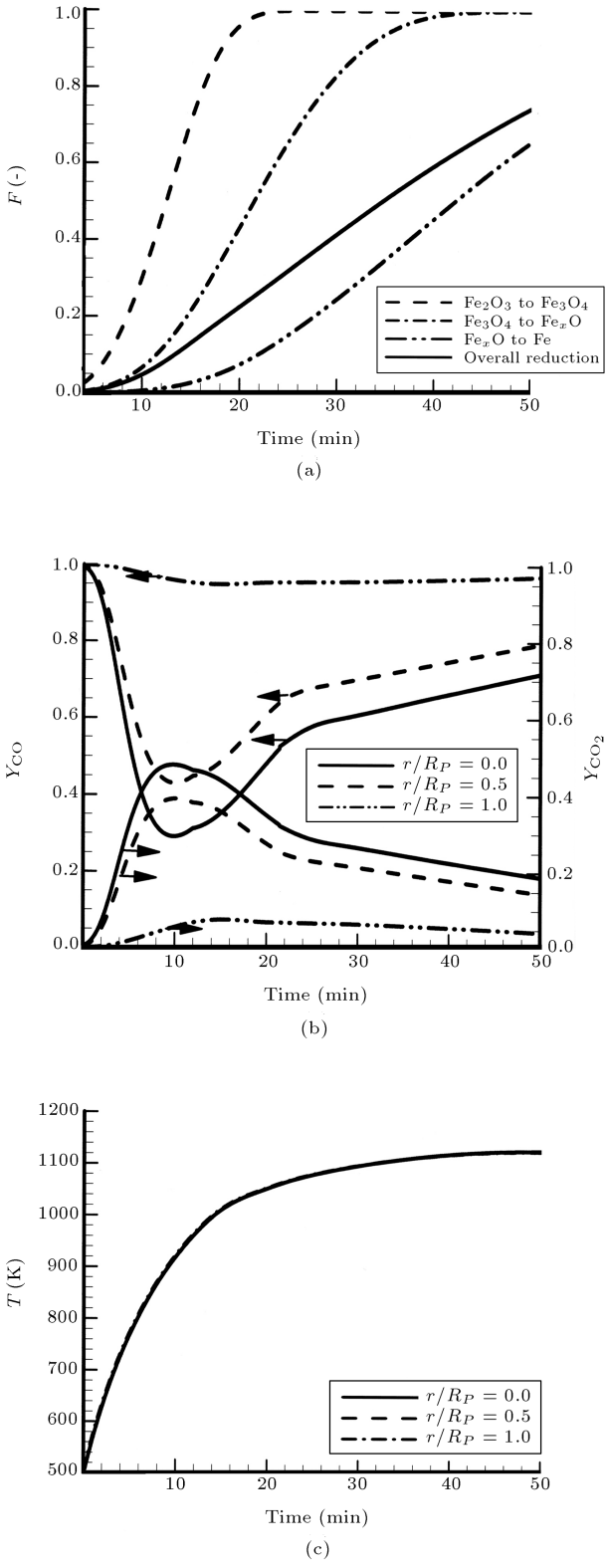

Figure 9. The model estimation of non-isothermal reduction of the pellet Type B with using pure carbon monoxide: (a) Overall reduction rate and reduction rate of each iron oxide component; (b) Gaseous reactant and product variation in three different positions within the pellet during the reduction; (c) Temperature variation in three different positions inside the pellet.

and 10d, that the temperature distribution inside the pellet is independent of position and varies by the time throughout the pellet simultaneously. In other words there is no temperature distribution within the pellet due to endo-or exothermic reactions, because of the dominant effect of thermal diffusion.

Figure 11 shows a comparison of the temperature variation during the reduction of a Type B hematite pellet with hydrogen, carbon monoxide and Syngas. It is observed that the temperature of the pellet rapidly approaches the bulk flow temperature when hydrogen is used as the reducing gas, and the temperature slowly approaches the bulk flow temperature when carbon monoxide is applied as a reducing gas, and the temperature approaches the bulk flow temperature, intermediately when the pellet is reduced by Syngas. However, for reduction by carbon monoxide, the temperature of the pellet is raised more than bulk flow temperature due to the highly exothermic reaction of the wustite conversion.

Figures 12a, 12b and 12c show a comparison between the overall reduction rates of pellet Type B by hydrogen, carbon monoxide and Syngas, respectively. They indicate that the isothermal reduction rate is higher than the nonisothermal reduction rate in all cases, because in the isothermal case the rate of reactions is higher than that in the non-isothermal case.

Effect of Gas Ratio and Gas Utility

In industrial reduction processes, the gas ratio ($\beta = \frac{H_2}{CO}$) commonly varies in the range of $0 < \beta < 4.0$, and the gas utility ($\gamma = \frac{(H_2+CO)}{(H_2O+CO_2)}$) may change in the range of $5 < \gamma < 49$, depending on the gas reforming system [38]. Figure 13a shows the model estimation of the non-isothermal reduction of pellet Type B using Syngas with constant gas utility, $\gamma = 8.71$, in which the gas ratio (β) has been varied in the range $0.5 < \beta < 3.5$. It can be observed that the reduction rate is increased as the gas ratio is raised. However, it is indicated in Figure 13b that the effect on the rate of reduction is not considerable when the gas ratio is raised above $\beta = 2.0$.

The effect of reducing gas utility (γ) on the reduction rate is illustrated in Figure 14. The degree of reduction is diminished as the gas utility is lowered. However, there is no significant effect on the reduction rate (shown in Figure 14b) when the gas utility is increased above $\gamma = 15$.

CONCLUSION

A non-isothermal mathematical model of the reduction of a hematite pellet was developed. The results of this model are in good agreement with the experimental

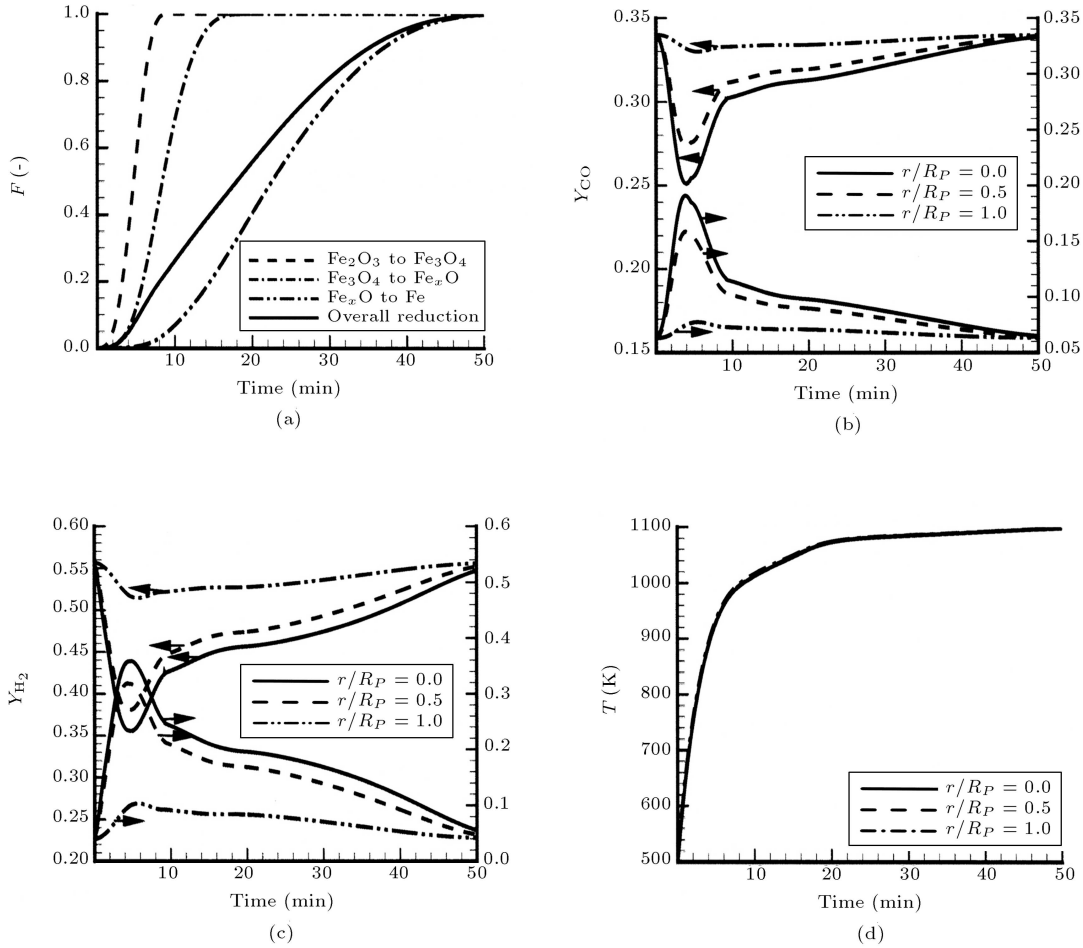

Figure 10. The model estimations of non-isothermal reduction of the pellet Type B with using Syngas: (a) Overall reduction rate and reduction rate of each iron oxide component; (b) and (c) Gaseous reactants and products variation at three different positions within the pellet during the reduction; (d) Temperature variation at three different positions inside the pellet.

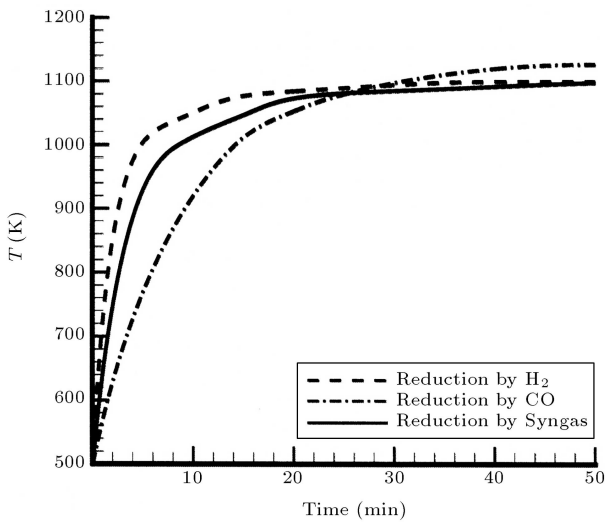

Figure 11. Temperature variation at $r = 0$ within the pellet during the reduction of the pellet Type B by pure hydrogen, pure carbon monoxide and Syngas.

data reported by Bonalde et al. [24]. The model was then applied to study nonisothermal reduction and the effect of gaseous composition on the reduction rate. It has been observed that the temperature of the pellet changes with the time of reduction due to endo- or exothermic reactions, in an isothermal condition. In isothermal and nonisothermal reduction there was no radial temperature distribution inside the pellet. In other words the temperature of the pellet changes due to the heat of reactions and the effective heat capacity of the pellet. In non-isothermal reduction the results of model application have revealed that any increase in gas utility (γ) will cause an improvement in the rate of reduction. However, the effect of the gas utility on the rate of reduction diminishes as the gas utility is increased above $\gamma = 15$. Also, a decline in gas ratio (β) may lead to a considerable decrease in the reduction rate of the pellet. On the other hand the effect of gas ratio on the rate of reduction is weakened as the gas ratio is raised above $\beta = 2$.

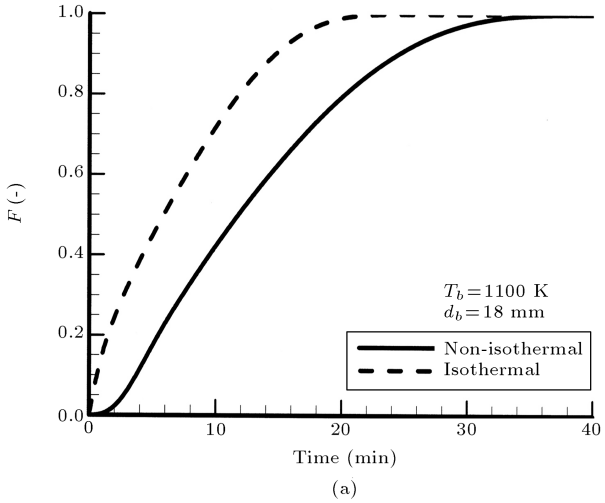

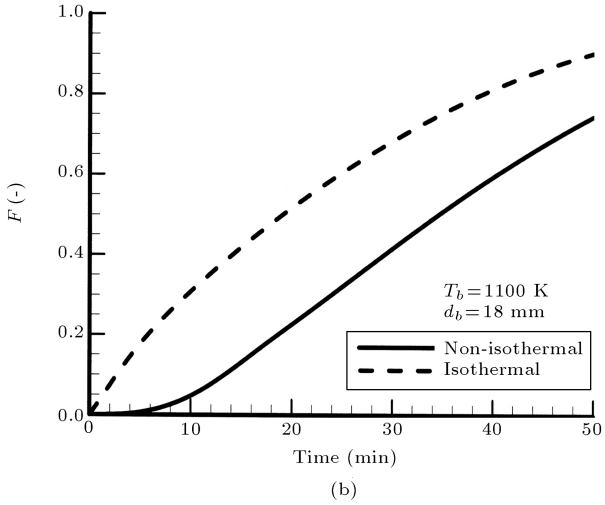

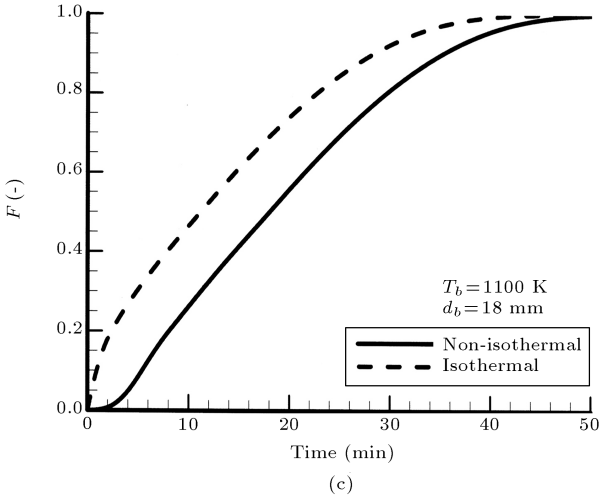

Figure 12. Comparison of non-isothermal and isothermal overall reduction rate of the pellet Type B: (a) Using pure hydrogen; (b) Using pure carbon monoxide; (c) Using Syngas with gas ratio ($\beta = 1.64$).

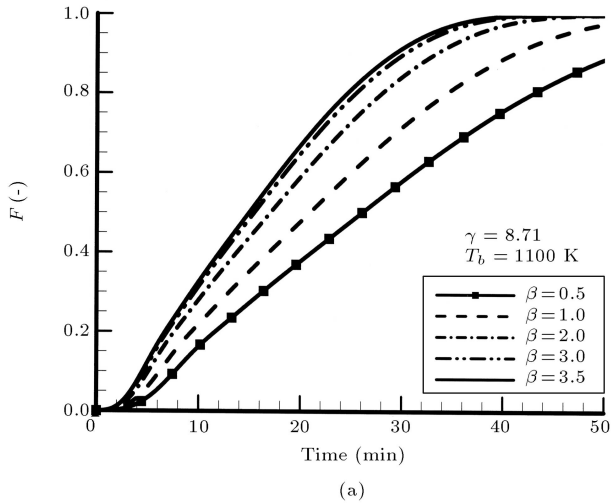

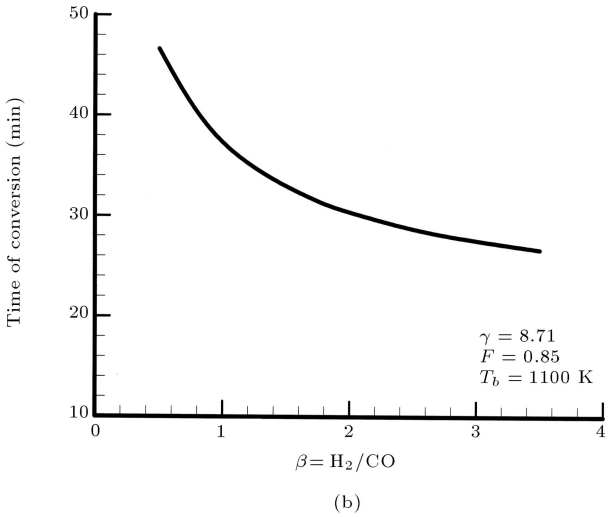

Figure 13. Non-isothermal reduction of the pellet Type B by Syngas with gas utility of $\gamma = 8.71$ and bulk temperature, $T_b = 1100$ K: (a) Reduction degree vs. time for different gas ratio (β); (b) Time required for 85 percent reduction of the pellet vs. gas ratio (β).

NOMENCLATURE

C_i	concentration of the ith component of the reducing gas (mol/m^3)
C_i^e	concentration of the ith component of the reducing gas at equilibrium condition (mol/m^3)
C_p	specific heat at constant pressure (J/kg.K)
D	diffusivity of gaseous species (m^2/s)
D_{ij}	binary diffusivity (m^2/s)
$d_{O,l}$	molar density of the reducible oxygen within the pellet (g-atom O/m^3)

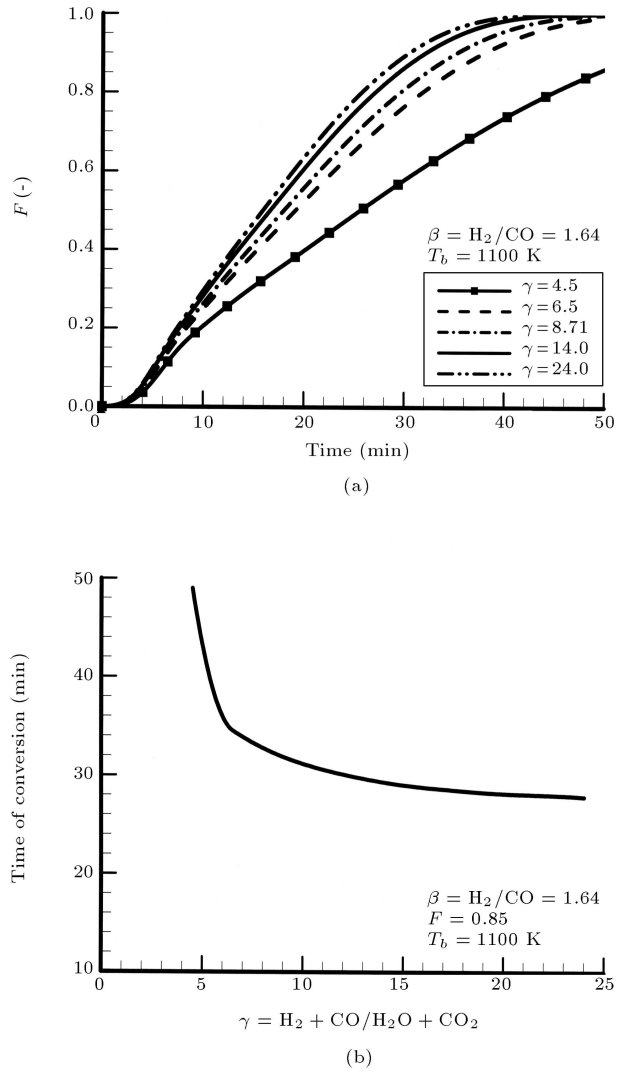

Figure 14. Non-isothermal reduction for the pellet Type B by Syngas with gas ratio, $\beta = 1.64$ and bulk temperature, $T_b = 1100$ K: (a) Reduction degree vs. time for different value of gas utility (γ); (b) Time required for 85 percent overall reduction of the pellet vs. gas utility parameter (β).

$Ea_{i,l}$	activation energy of the reaction with the ith component at interface l (kJ/mol)
f_l	local fractional reduction of the lth iron oxide component (-)
f	total local fractional reduction (-)
$(-\Delta H)_{T,i,l}$	heat of reaction with the ith gas component at interface l at temperature T (J/mol)
h	convective heat transfer coefficient (W/m^2.K)
$k_{r,i,l}$	reaction rate constant for reaction of the ith species at interface l (m/s)
$k_{o,i,l}$	frequency factor of reaction with the ith component at interface l (m/s)
$k_{f,i}$	mass transfer coefficient of the ith species through gaseous film (m/s)
$Ke_{i,l}$	equilibrium constant of reaction with the ith component at interface l (-)
M	molecular weight (g/mol)
Nu	Nusselt number ($= hd_P/\lambda_g$)
P_b	bulk flow pressure (bar)
P_t	total flow pressure (bar)
Pr	Prandtl number ($= \mu_g C_{pg}/\lambda_g$)
R_P	pellet radius (m)
R_G	universal gas constant (J/mol°K)
Re	Reynolds number ($= d_P \rho_g u_b \mu_g^{-1}$)
r	radial coordinate in the pellet (m)
r_g, r_l	radii of the grain and reaction interface within the grain respectively (m)
Sc	Schmidt number ($= \mu_g \rho_g^{-1} D_{\text{eff}}^{-1}$)
Sh	Sherwood number ($= d_P k_m D_{\text{eff}}^{-1}$)
t	time (s)
T	temperature (K)
$\dot{v}_{i,l}$	rate of chemical reaction with the ith gaseous species at interface l (mol/m^{2}s)
Y_i	mole fraction of the ith component of the reducing gas (-)
α_l	reducible oxygen at each step of reduction (-)
β	reducing gas ratio ($= H_2/CO$)
γ	reducing gas utility ($= (CO+H_2)/(CO_2+H_2O)$)
ρ	mass density (kg/m^3)
ε	porosity of the pellet (-)
λ	thermal conductivity (W/m.K)

Subscripts

i	related to gaseous component
l	related to reduction interfaces
s	related to solid (iron oxides)
g	related to Syngas
eff	effective parameters
b	related to bulk flow of Syngas
t	related to total value of parameter
h, m, w	related to hematite-magnetite, magnetite-wustite and wustite-iron interface, respectively
0	related to initial value of parameters

Superscripts

k	related to Knudsen diffusivity
m	related to molecular diffusivity

REFERENCES

1. McKewan, W.M. "Kinetics of iron oxide reduction", *Transaction of the American Institute of Mining and Metallurgical Engineers*, **218**, pp. 2-6 (1960).
2. McKewan, W.M. "Reduction kinetics of magnetite in H_2-H_2O-N_2 mixtures", *Transaction of Metallurgical Society of AIME*, **221**, pp. 140-145 (1961).
3. McKewan, W.M. "Reduction kinetics of hematite in hydrogen-water vapor-nitrogen mixtures", *Transaction of Metallurgical Society of AIME*, **224**, pp. 2-5 (1962).
4. Turkdogan, E.T. and Vinters, J.V. "Gaseous reduction of iron oxides: Part I. Reduction of hematite in hydrogen", *Metallurgical Transactions*, **2**, p. 3175 (1971).
5. Turkdogan, E.T. and Vinters, J.V. "Gaseous reduction of iron oxides: Part III. Reduction-oxidation of porous and dense iron oxides and iron", *Metallurgical Transactions*, **3**, p. 1561 (1972).
6. Turkdogan, E.T., Olsson, R.G. and Vinters, J.V. "Gaseous reduction of iron oxides: Part II. Pore characteristics of iron reduced from hematite in hydrogen", *Metallurgical Transactions*, **2**, p. 3189 (1971).
7. Szekely, J. and El-Tawil, Y. "The reduction of hematite pellets with carbon monoxide-hydrogen mixtures", *Metallurgical Transactions B-Process Metallurgy*, **7**, pp. 490-492 (1983).
8. Towhidi, N. and Szekely, J. "Reduction kinetics of commercial low-silica hematite pellets with CO-H_2 mixtures over temperature range 600-1234°C", *Ironmaking and Steelmaking*, **6**, pp. 237-249 (1981).
9. Towhidi, N. and Szekely, J. "The influence of carbon deposition on the reduction kinetics of commercial grade hematite pellets with CO, H_2 and N_2", *Metallurgical Transaction B*, **14**, pp. 359-367 (1983).
10. Paul, S. and Mukherjee, S. "Non-isothermal and isothermal reduction kinetics of iron ore agglomerates", *Ironmaking and Steelmaking*, **19**, pp. 190-193 (1992).
11. Proctor, M.J., Hawkins, R.J. and Smith, J.D. "Reduction of iron ore pellets in CO-CO_2-H_2-H_2O mixtures", *Ironmaking and Steelmaking*, **19**, pp. 194-200 (1992).
12. Janowski, J. and Sadowski, A. "Kinetics of low temperature reduction of hematite to magnetite", *Ironmaking and Steelmaking*, **23**, pp. 479-485 (1996).
13. Moon, I.J., Rhee, C.H. and Min, D.J. "Reduction of hematite compacts by CO-H_2 gas mixtures", *Steel Research*, **69**, pp. 302-306 (1998).
14. Kang, H.W., Chung, W.S. and Murayama, T. "Effect of iron ore size on kinetics of gaseous reduction", *ISIJ International*, **38**, pp. 109-115 (1998).
15. Kang, H.W., Chung, W.S., Murayama, T. and Ono, Y. "Effect of iron ore shape on gaseous reduction rate", *ISIJ International*, **38**, pp. 1194-1200 (1998).
16. Spitzer, R.H., Manning, F.S. and Philbrook, W.O. "Mixed-control reaction kinetics in the gaseous reduction of hematite", *Transaction of the Metallurgical Society of AIME*, **236**, pp. 726-742 (1966a).
17. Spitzer, R.H., Manning, F.S. and Philbrook, W.O. "Generalized model for the gaseous, topochemical reduction of porous hematite spheres", *Transaction of the Metallurgical Society of AIME*, **236**, pp. 1715-1724 (1966b).
18. Tien, R.H. and Turkdogan, E.T. "Gaseous reduction of iron oxides: Part IV. Mathematical analysis of partial internal reduction-diffusion control", *Metallurgical Transactions*, **3**, p. 2039 (1972).
19. Tsay, Q.T., Ray, W.H. and Szekely, J. "The modelling of hematite reduction with hydrogen plus carbon monoxide mixtures. Part I. The behaviour of single pellets", *AIChE J.*, **22**, pp. 1064-1079 (1976).
20. Hara, Y., Sakawa, M. and Kondo, S. "Mathematical model of the shaft furnace for reduction of iron ore pellet", *Tetsu-to-Hagane*, **62**, p. 315 (1976).
21. Negri, E.D., Alfano, O.M. and Chiovetta, M.G. "Direct reduction of hematite in a moving bed. Comparison between one- and three interface pellet models", *Chemical Engineering Science*, **42**, pp. 2472-2475 (1987).
22. Yu, K.O. and Gillis, P.P. "Mathematical simulation of direct reduction", *Metallurgical Transactions B*, **12**, p. 111 (1981).
23. Usui, T., Ohmi, M. and Yamamura, E. "Analysis of rate of hydrogen reduction of porous wustite pellets based on zone reaction models", *ISIJ International*, **30**, pp. 347-355 (1990).
24. Bonalde, A., Henriquez, A. and Manrique, M. "Kinetic analysis of the iron oxide reduction using hydrogen-carbonmonoxide mixtures as reducing agent", *ISIJ International*, **45**, pp. 1255-1260 (2005).
25. Szekely, J. and Evans, J.W. "A structural model for gas-solid reactions with moving boundary-II the effect of grain size, porosity and temperature on the reaction of porous pellets", *Chemical Engineering Science*, **26**, pp. 1901-1913 (1971).
26. Valipour, M.S., Kuwabara, M. and Saboohi, Y. "Numerical modeling of non-isothermal reduction in a hematite pellet with using a mixture of H_2, H_2O, CO and CO_2", *CAMP-ISIJ*, **18**, p. 922 (2005).
27. Valipour, M.S., Motamed Hashemi, M.Y. and Saboohi, Y. "Mathematical modelling of reaction in an iron ore pellet with using a mixture of hydrogen, water vapor, carbon monoxide and carbon dioxide: An isothermal study", *Advanced Powder Technology*, **17**, pp. 277-295 (2006).
28. Valipour, M.S. and Saboohi, Y. "Modeling of multiple noncatalytic gas-solid reactions in a moving bed of Porous pellets based on finite volume method", *Heat and Mass Transfer*, **43**, pp. 881-894 (2007).

29. Shi, J., Donskoi, E., McElwain, D.L.S. and Wibberley, L.J. "Modelling the reduction of an iron ore-coal composite pellet with conduction and convection in an axisymmetric temperature field", *Mathematical and Computer Modelling*, **42**, pp. 45-60 (2005).

30. Akiyama, T., Takahashi, R. and Yagi, J. "Measurements of heat transfer coefficients between gas and particles for a single sphere and for moving beds", *ISIJ International*, **33**, pp. 703-710 (1993).

31. Fuller, E.N., Schettler, P.D. and Giddings, J.C., *Indust. and Eng. Chem.*, **58**, p. 19 (1966).

32. Geiger, G.H. and Poirier, D.R., *Transport Phenomena in Metallurgy*, Addison-Wesey, NewYork (1980).

33. Valipour, M.S. "Numerical modeling of iron oxides reduction in a midrex shaft furnace", PhD Thesis, Sharif University of Technology, Tehran, Iran (2007).

34. Donskoi, E. and McElwain, D.L.S. "Estimation and modelling of parameters for direct reduction in iron ore/coal composites: Part I. physical parameters", *Metallurgical and Materials Transactions B*, **34B**, pp. 93-102 (2003).

35. Akiyama, T., Ohta, H., Takahashi, R., Waseda, Y. and Yagi, J. "Measurement and modeling of thermal conductivity for dense iron oxide and porous iron ore agglomerates in stepwise reduction", *ISIJ International*, **32**, pp. 829-837 (1992).

36. Muchi, I., Asai, S. and Kuwabara, M. "Principles of chemical and metallurgical reaction engineering", in *Advances in Transport Process in Metallurgical Systems*, Chapter 2, Y. Sahai and G.R.S.T. Pierre, Eds., Elsevier, Tokyo (1993).

37. Versteeg, H.K. and Malalasekera, W., *An Introduction to Computational Fluid Dynamics: The Finite Volume Method*, Addison-Wesley, Reading (1995).

38. Takenaka, Y., Kimura, Y., Narita, K. and Kaneko, D. "Mathematical model of direct reduction shaft furnace and its application to actual operations of a model plant", *Computers and Chemical Engineering*, **10**, pp. 67-75 (1986).